Direct Observation of Conformations of a High-Mobility n‑Type Low-Bandgap Copolymer in Solutions and Solid Films

Xinmao Li, Jianxin Guan, Chengzhen Shen, et al.

View Online   **Export Citation**   **CrossMark**

ARTICLES YOU MAY BE INTERESTED IN

Direct Observation of Conformations of a High-Mobility n-Type Low-Bandgap Copolymer in Solutions and Solid Films

Xinmao Li, Jianxin Guan*, Chenzhen Shen, Zhihao Yu, Junrong Zheng*

College of Chemistry and Molecular Engineering, Beijing National Laboratory for Molecular Sciences, Peking University, Beijing 100871, China

*Corresponding Email: junrong@pku.edu.cn (J.Z.), guanjianxin1125@pku.edu.cn (J.G.)

Abstract

The aggregation morphologies of conjugated polymers in solutions and solid films are important for their optoelectronic applications. Due to the amorphous state of the polymers, it remains a great challenge to determine their conformations in either liquids or solids. Herein, a ps/fs synchronized 2D IR technique is applied to investigate the molecular conformations of a high-mobility n-type low-bandgap copolymer N2200 dissolved in $CHCl_3$ and CCl_4 and in solid films cast from both solutions by the vibrational cross angle method. In CCl_4 the polymer forms more aggregates and folds more and the backbone dihedral angle of C-C(NDI)/C-S(Thiophene) of its average conformation is about 10° more distorted than that in $CHCl_3$ and the most stable conformation for a free molecule. Anti-intuitively, the solid films cast from both solutions have the same molecular conformation, and the conformation is similar to that in the polar $CHCl_3$ rather than the conformation in the less polar CCl_4. The results imply that the interaction between the polymer backbones is probably stronger than its interaction with CCl_4, which can naturally guide the rearrangement of polymer chains during the evaporation of solvent molecules. This work also implies that the balance and competition between the polymer/polymer interaction and the polymer/solvent interaction seems to be the dominant factor responsible for what morphology can form in a solid film cast from solution. It is not always true that different molecular conformations must exist in solid films grown from different solutions with different polarity or different extents of aggregates with different conformations.

I.   Introduction

Conjugated polymers have been extensively used as photoelectric materials in organic photovoltaic (OPV) devices, organic field-effect transistors (OFETs) and bioelectronics and many other fields because of many desirable properties, e.g. high-throughput solution processibility, chemical diversity, self-healing properties and mechanical flexibility.([1-3]) The microstructure of conjugated polymers is deemed to be one key factor that determines their device performance. For examples, the backbone torsional angles can increase conformational disorder and decrease effective conjugation length and thus alter intrachain charge transports.([4]) When polymer chains interact to form aggregates, the π-orbitals of adjacent chains can stack coplanar, providing a pathway for inter-chain charge transport. Experimental results have suggested that the twisting and aggregation of polymers can significantly affect their properties.([5-10])

Many high-mobility conjugated polymers have been suggested to form aggregates in organic solvents due to strong interchain $\pi - \pi$ interactions,([11-13]) and the aggregation behavior of conjugated polymers in solution plays an important role in the solid-state microstructure that determine their photoelectric performance.([14-16]) Some studies even suggest that the thin film morphology of conjugated polymers can inherit the supramolecular characteristics of their solution states.([17]) Regulating the aggregation of conjugated polymers in solution is suggested to be an effective way to tune the microstructure and physical properties of the solid state.([18-20]) Consequently, understanding the aggregation behavior and conformations of conjugated polymers in solution is of significance for tailoring their device performance. However, the aggregation structure and conformations of most previously reported conjugated polymer solutions were only indirectly derived from light and x-ray scattering, UV-Vis absorption, photoluminescence and 1D NMR, combined with theoretical calculations([17, 21-24]). Direct determination of aggregates' conformational details in solutions at the molecular level remains a grand challenge, so as the correlation between conformations in liquids and solids.

N2200 is a typical n-type polymer, which exhibits a large electron field-effect mobility of up to 0.85 cm^2/Vs.([25]) Its film morphology or texture and its solution-state supramolecular structures have been intensely explored.([21-24]) By detailed steady-state UV-Vis, photoluminescence, NMR and quantum chemical calculations, Neher and co-workers reveal distinct signatures of N2200 aggregation in its solutions: in nonpolar solvents such as toluene, N2200 exists in a aggregated form, whereas in chloronaphthalene it is dispersed as a single chain. Although the calculation results show that the skeleton and thiophene chain of the molecule have different torsion angles under different aggregation states, there is no specific experimental support. In addition, in other solvents, another form of aggregation is speculated to exist based on absorption spectra, but lack of experimental evidence to describe its conformation or structure.([24])

Two-dimensional infrared (2D IR) is an ultrafast coherent vibrational spectroscopic technique that has found broad use in studies of kinetics, hydrogen bonding and molecular structure.([26-43]) In a two-dimensional infrared spectrum, cross-peaks (off-diagonal peaks) can be used to determine the coupling between vibration modes, and their anisotropy values directly reflect the relative angle of the transition dipoles of two coupled vibrations. In principle, it is feasible to determine the molecular conformations and even the morphology of aggregates by 2D-IR if the number of experimentally determined vibrational cross angles is sufficiently large.([44-47]) However, the coupling signal between vibrations with relatively small transition dipole moments (e.g. C-H stretches and bending) can be too small to be detected if excited with a broadband femtosecond (fs) pulse. This is because the energy of a fs pulse is typically distributed in the range of 150-300 cm^{-1} wide, whereas the typical band width of a vibration is 10-40 cm^{-1} (except OH and NH stretches and other modes which can form strong H-bonds). Most of the laser energy is not used when a fs pulse is applied to excite a narrow-banded vibration. To improve the excitation energy and still maintain a fs temporal resolution, a 2D IR technique that synchronizes a picosecond (ps) laser and a fs laser was developed([48]).   The ps laser (~1.5 ps) provides a narrow bandwidth of 10~30 cm^{-1} so that most of the pulse energy can be used in

vibrational excitations, and the fs laser provides a broadband detection.(*44, 49*) With such a technical setup, many weak vibrational couplings can be detected and three-dimensional conformations of a molecule can be mapped.(*44, 48*)

Herein, using the synchronized ps-fs 2D IR technique, we acquire 2D IR spectra of N2200 in carbon tetrachloride (CCl_4) and chloroform ($CHCl_3$) and the solid state, respectively. The two solvents are chosen for the study because they have relatively few spectrally overlapped vibrational peaks with N2200 and a large solvation difference for N2200(*24*). Combined with theoretical calculations and anisotropy, the experimental results reveal different conformations of N2200 in the samples.

II.   Experimental Methods

The optical setup was described previously.(*44, 49*) Briefly, a picosecond amplifier and a femtosecond amplifier are synchronized with the same seed pulse (Aria-Ti oscillator, Phidia-ps and Phidia-fs amplifiers, Uptek Solutions). The picosecond amplifier pumps an optical parametric amplifier (OPA-ps, Light Conversion) to produce ~1.3 ps mid-IR pulses with a bandwidth of ~13 cm^{-1}. The femtosecond amplifier pumps another OPA (Palitra, Quantronix) to produce ~60 fs mid-IR pulses with a bandwidth of ~200 cm^{-1} in a tunable frequency range from 1300 to 3500 cm^{-1}. In 2D-IR and pump/probe experiments, the picosecond IR pulse is the excitation beam. The femtosecond IR pulse is the detection beam, which is frequency resolved by a 2 × 64 pixel mercury cadmium telluride (MCT) detector (Infrared System) (resolution is 1~3 cm^{-1}, dependent on the frequency), yielding the detection axis of the 2D-IR spectrum. The temporal shapes of the IR pulses are mostly Gaussian (see Figure S1 in Supporting Information, SI). Scanning the excitation frequency yields the other axis of the spectrum. Two polarizers are added into the detection beam path to selectively measure the parallel or perpendicular polarized signal relative to the excitation beam. Measuring the transmission of the mid-IR beam through the sample by chopping the excitation beam at 500 Hz, the pump-probe signal *I(t)* is collected and the vibrational lifetimes are obtained from the rotation-free signal:

$$I(t) = \ (I_{\parallel}(t) + 2\,I_{\perp}(t))\,/\,3. \qquad\qquad \text{eq.1}$$

The M_w and polydispersity of the polymer is determined to be 63.7 kDa and 2.07, respectively (GPC result is provided in Fig.S11). The concentration of the sample is 10 mg/mL, and samples for the FTIR, 2D-IR measurements are contained in sample cells composed of two CaF_2 windows separated by a 100 μm thick Teflon spacer. For optical investigations on N2200 films, solutions are coated directly onto CaF_2 windows and dried under the ambient condition without further treatments.

Geometry optimizations and vibrational frequency of trimer and octomer calculation are carried out using density functional theory (DFT) with the B3LYP functional employing the 6-31G (d).

III.   Results
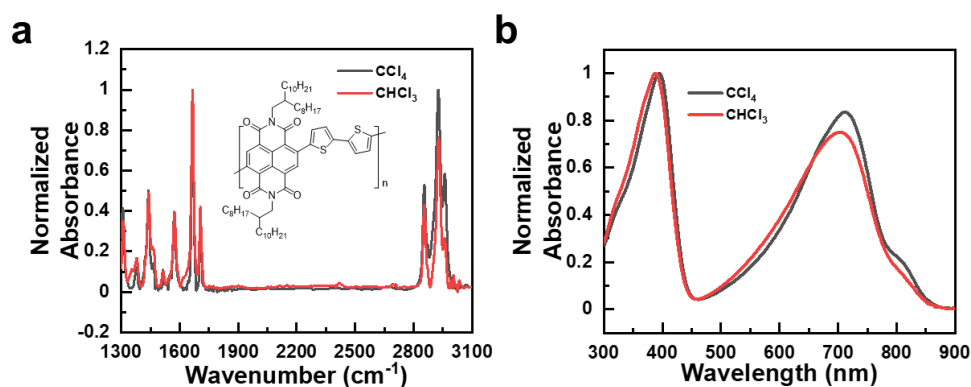
III.1   FTIR and UV-Vis absorption spectra

Fig.1 (a) FTIR and (b) UV-Vis absorption spectra of N2200 in $CHCl_3$ (red) and CCl_4 (black) solutions, respectively. The concentration of both samples is 10 mg/mL.

Fig.1 displays the FTIR and UV-Vis absorption spectra of N2200 in two solvents, $CHCl_3$ and CCl_4. The peak positions in FTIR spectra (Fig.1a) in the two solutions are similar, whereas the shapes and relative intensities of some peaks are different, which can generally be attributed to different solvations. In order to better assign the vibration peaks, we optimize the structure of N2200 octomer and calculate different vibrations on the skeleton, and the vibration of the side chain is given by calculation of the monomer. According to calculations, the major vibrational peaks in the FTIR spectrum (Fig.1a) are assigned as follows: C-H wagging on thiophene (1308 cm^{-1}), thiophene

6

skeleton stretch (1440 cm^{-1}), NDI skeleton stretch (1572 cm^{-1}), C=O stretch (ν_{as-1}: 1665 cm^{-1}, ν_{as-2}:1705 cm^{-1}) and a series of C-H stretches ranging from 2855 cm^{-1} to 2960 cm^{-1}. The UV-Vis absorption peaks of N2200 in the two solvents CHCl$_3$ and CCl$_4$ (fig.1b) are different. Both π-π* UV band at about 400 nm and the low energy charge transfer transition peak at about 700 nm red shift when decreasing the polarity of the solvent from CHCl$_3$ to CCl$_4$, and a new shoulder appears at about 800 nm. The spectral difference in the two solvents could be partially attributed to solvatochromism([50, 51]), but further temperature and molecular weight experiments([24]) have suggested that the aggregation between the polymer chain or chain segments plays a vital role to the observed absorption change. Higher concentrations can potentially increase intermolecular aggregation. However, the absence of spectral concentration dependence suggests that the aggregation of N2200 is primarily an intra-chain behavior. (Fig. S2) Previous reports have shown that N2200 (1) in non-polar solvents such as toluene, aggregates and stacks better than in polar solvents, and (2) dissolves as a dispersed single strand polymer in chloronaphthalene.([24]) However, in solvent with a medium polarity, such as chloroform, the aggregation state is not reported. In general, peak shifts, spectral broadening, and the appearance of new features of a polymer solution are most likely caused by morphology changes.([52, 53]) Accordingly, it is likely that N2200 is better solvated by chloroform so that aggregation and stacking are not as severe as in CCl$_4$.
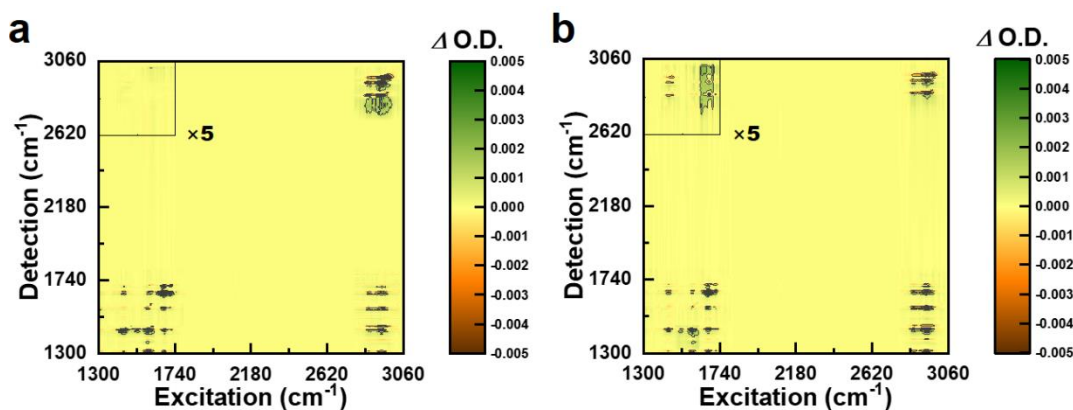
III.2   2D IR spectra

Fig.2 2D-IR spectrum of N2200 in CCl$_4$ ranging from 1300 cm^{-1} to 3500 cm^{-1} at waiting time of 0.3 ps (a) and 3 ps (b). The relative peaks are adjusted to be more comparable.

The structural details of conformation and aggregation differences of N2200 in the two solutions are difficult to be obtained from FTIR measurements in Fig.1a, because the frequencies and shapes of vibrational peaks are affected not only by molecular structures but also accidental degeneracies. 2D IR spectra of N2200 in the solutions are therefore collected to investigate the structural origins for the electronic transition differences observed in fig.1b in the two solutions. Fig.2 displays 2D-IR spectra of N2200 in CCl_4 in the range of 1300 cm^{-1} to 3060 cm^{-1} at two different waiting times. Many diagonal and cross peak pairs appear in the spectra. The red peak of a diagonal peak pair is from the 0-1 transition of a vibration mode, and the blue peak is from its 1-2 transition. The y-axis frequency of the red peak corresponds to its 0-1 transition frequency, which is identical to its x-axis frequency and the frequency measured with FTIR. The y-axis frequency of the blue peak corresponds to its 1-2 transition frequency, which is typically smaller than the 0-1 frequency because of anharmonicity. A cross peak pair also contains a red peak and a blue peak, originating from the coupling between two vibrations: after one vibration is excited with frequency in the x-axis, the excitation of this vibration shifts the 0-1 transition frequency of another mode because they are coupled. Typically, a vibrational excitation redshifts coupled vibrational transition frequencies, resulting in a bleaching (red peak) in the 0-1 transition of the coupled mode and a new absorption (blue peak) of the redshifted 0-1 transition frequency. The vibrational coupling anharmonicity between two vibrational modes is manifested by the y-axis position difference of the off-diagonal peak pair. The relative orientations of the two coupled vibrational modes can be obtained from the polarization-selective measurements of the off-diagonal peak intensities, which will be our focus of data analysis.
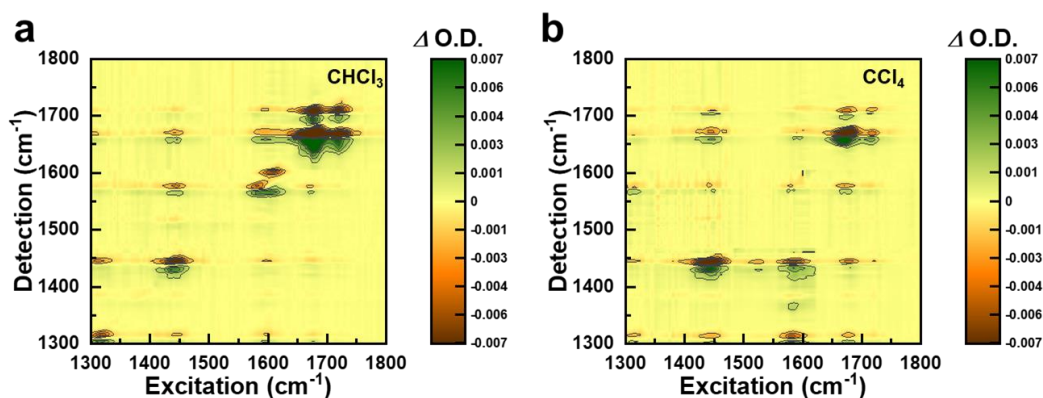
8

Fig.3 2D-IR spectrum of N2200 in CHCl3 (a) and CCl4 (b) at a waiting time of 0.3 ps.

Fig.3 displays 2D-IR spectra of N2200 in CHCl3 and CCl4 at a waiting time of 0.3 ps. Three salient differences appear in the two solutions. First of all, in CHCl3, the C=O stretch peaks (1650 ~ 1720 cm^{-1}) are obviously broader than in CCl4, because CHCl3 is more polar and interacts stronger with the C=O bond. A similar phenomenon was previously observed in metal carbonyl compounds dissolved in CHCl3 and hexane.(*54*) Second, a much stronger diagonal peak at about 1617 cm^{-1} appears in CHCl3 than in CCl4. Similarly, the NDI skeleton stretching (1572 cm^{-1}) is also much stronger in CHCl3. In FTIR spectra in fig.1a (also the enlarged spectrum in fig.S6 in SI), the peak at about 1617 cm^{-1} is also larger in CHCl3, but much smaller than the NDI skeleton stretching peak in either solvent, and the NDI skeleton stretching peaks in both solutions have similar intensities. The difference in relative peak intensity comes from the fact that the 2D IR signal is proportional to the fourth power of the transition dipole moment, whereas the FTIR signal is proportional to the transition dipole moment square. The peak at 1617 cm^{-1} is a Fermi resonance of a dark mode with the C=O stretching and with the NDI skeleton stretching modes, which mixes the transition dipole moments of the three coupled modes because of the linear combination of the local modes.(*55*) In CCl4, the Fermi resonance peak also exists, but with a lower frequency at about 1603 cm^{-1}. Since this is 14 cm^{-1} further away from the C=O stretch (compared to in CHCl3), its ability to "borrow" intensity from C=O stretch is much weaker (the coefficient of the C=O local mode in the linear combination is smaller).(*55*) This phenomenon that the intensities of Fermi resonance peaks are significantly changed by solvents is not

9

unusual. It was previously observed in a series of alkyl isocyanate compounds (R-N=C=O).(*56*) Third, the thiophene skeleton stretch peak (1440 cm^{-1}) is smaller in CHCl$_3$. This is somewhat surprising. If the thiophene is equally solvated in both solutions, one would expect the thiophene skeleton stretch to be stronger in CHCl$_3$, similar to the C=O stretch because of the stronger interaction of the polar CHCl$_3$. One possible explanation for this seeming abnormal observation is that in CCl$_4$ the polymer is less solvated and more aggregates form, leading to more stacking of the thiophene pi electrons(*57*) and an enhanced transition dipole moment of the thiophene skeleton stretch vibration. Nevertheless, although all the experimental results discussed above suggest that the polymer morphology can be different in the two solvents, none of them is definitely evident.

III.3   Vibrational cross angle analysis

In order to further investigate the molecular structural details in the solutions, we analyze the cross angles between coupled vibrations measured with polarization-selective experiments. As mentioned above, the intensity of the off-diagonal peak pairs depends on the polarizations of the excitation and detection beams. The cross angle of the transition dipoles of two coupled vibrations can be calculated from experimentally measured signal anisotropy:

$$R = (I_\parallel - I_\perp)/(I_\parallel + 2I_\perp), \qquad \text{eq.2}$$

where $I_\parallel$ and $I_\perp$ are the off-diagonal intensities with parallel and perpendicular excitation/detection polarizations, respectively. According to the relationship between the anisotropy (R) of the coupled vibrations and the cross angle (θ) between their transition dipole moments:

$$R = \frac{3cos^2\theta - 1}{5}, \qquad \text{eq.3}$$

the angle (θ) between different transition dipole moments can be obtained. In order to avoid the influence of molecular rotation, energy transfer or heat induced bleaching on the results, the blue cross peaks at a waiting time of 0 ps are selected to calculate the anisotropy.(*48*)

The anisotropy values and vibrational cross angles between 1300-1800 cm^{-1} are

listed in Table 1, and the corresponding pump/probe data (parallel and perpendicular) for the 10 pair coupled modes are displayed in fig.S7 & S8 of SI. In the case of N2200, the flexible alkyl chains are located outside the skeleton and have a relatively random distribution, which is expected to have a relatively small effect on the skeleton packing. Therefore, our main focus is placed on the analysis of the main chain vibrations. In the NDI unit, the cross angles between the transition dipole moments of either C=O(ν_{as-1})/C=O(ν_{as-2}) pair or NDI skeleton/C=O(ν_{as-2}) pair are ~ 60°, independent of the solvent selection. However, the relative orientation between the NDI skeleton/C=O(ν_{as-1}) pair shows a difference of approximately 6°. It is ~ 24° in CCl$_4$ and ~ 30 ° in CHCl$_3$, respectively. The solvent dependence of vibrational cross angles is more salient between vibration modes of the NDI unit and the thiophene skeleton. In CCl$_4$, the cross angles of thiophene/NDI skeleton, thiophene skeleton/C=O stretching (ν_{as-2}), and thiophene skeleton/C=O stretching (ν_{as-2}) vibrations are 17°,30° and 55° respectively, whereas they are 24°, 23°, 49° in CHCl$_3$. The vibrational cross angles directly reflect the relative orientations between vibrational modes, which in turn are determined by the cross angles between chemical bonds. The experimentally observed different vibrational cross angles in CHCl$_3$ and CCl$_4$ suggest that the torsions and packing conditions of the polymer main chain are different in the two solvents.

Table 1. Anisotropy and vibrational cross angles of N2200 in CCl$_4$ and CHCl$_3$ at a waiting time of 0 ps.

Pair Number	Coupled modes	Anisotropy (CCl$_4$)	Cross angle(CCl$_4$)	Anisotropy(CHCl$_3$)	Cross angle(CHCl$_3$)
1	C-H / Thiophene Skeleton	0.16	39	0.17	38
2	C-H / NDI skeleton	-0.12	69	-0.15	73
3	C-H / C=O(ν_{as-1})	-0.1	66	-0.05	60
4	C-H / C=O(ν_{as-2})	0.25	30	0.25	30
5	Thiophene Skeleton / NDI skeleton	0.27	28	0.3	24
6	Thiophene Skeleton / C=O(ν_{as-1})	0.25	30	0.31	23
7	Thiophene Skeleton / C=O(ν_{as-2})	0	55	0.06	49
8	NDI skeleton / C=O(ν_{as-1})	0.3	24	0.25	30
9	NDI skeleton / C=O(ν_{as-2})	-0.08	63	-0.05	60
10	C=O(ν_{as-1}) / C=O(ν_{as-2})	-0.05	60	-0.07	62

The experimentally measured vibrations are normal modes, and thus the

vibrational cross angles are not the same as those cross angles between chemical bonds. However, one molecular conformation can only have one set of vibrational cross angles, and vice versa. Therefore, vibrational cross angles can be translated into molecular conformations, provided that the number of vibrational cross angles is larger than the bond degree of freedom.(*58*)

To convert vibrational cross angles into molecular conformations, the standard procedure is to first optimize molecular conformations preset by rotating along single bonds and then compare the calculated vibrational angles of each conformation to the experimental values. The conformation that gives vibrational angles closest to the experimental results is deemed to be the conformation determined by the method.(*58*) Considering that the alkyl chain is inessential to the conformation of molecular stacking, as explained above, the alkyl chain is omitted in calculations to reduce the computational burden. In addition, to save computational cost, instead of an entire polymer chain, only the conformations of a trimer with different torsion angles are calculated. The deviation Er's between the calculated and experimental vibrational cross angles are shown in fig.4. Er is defined as

$$Er = \frac{\sum_{i=5}^{10} |A_i^C - A_i^E|}{6}, \qquad \text{eq.4}$$

where A_i^C is the calculated vibrational cross angles of ith pair of normal modes. The computed vibrational modes of the trimer are complicated because of its large size. To minimize possible vibrational misassignments of the experimental IR peaks, only six cross angles of vibrations that have relatively large transition dipole moments and large contributions from the center NDI and thiophene units are chosen for analysis. A_i^E is the experimental value, listed in Table 1. As shown in fig.4, in $CHCl_3$, the calculation results based on either the energy minimum or experimental vibrational cross angles lead to the same most probable conformation with the dihedral angle of C-C(NDI)/C-S(Thiophene) ~38.5°. In CCl_4, this dihedral angle is ~10° larger (Fig. 5). The result implies that in CCl_4 the thiophene ring twists to a larger degree. In $CHCl_3$ the polymer chain is more planar and closer to the most stable conformation of a free molecule. It is known that $CHCl_3$ is a better solvent for the polymer than CCl_4. In a better solvent, a

polymer chain tends to extend better and have fewer folds and less distortion. When the polymer chain extends better, it is more like a free chain. The observed structural difference in $CHCl_3$ and CCl_4 is consistent with the general knowledge about polymer solution. Moreover, we also investigate the torsion between two NDI fragments. Interestingly, twisting the angle between two adjacent NDI fragments doesn't produce any obvious difference, as illustrated in fig.S9. From -10 to 10°, the optimal structure points to the same result as illustrated in fig.4. It is worth to not that it is likely that more than one polymer conformations exist in either solution, and what is analyzed above is the average structure rather than any particular conformation.
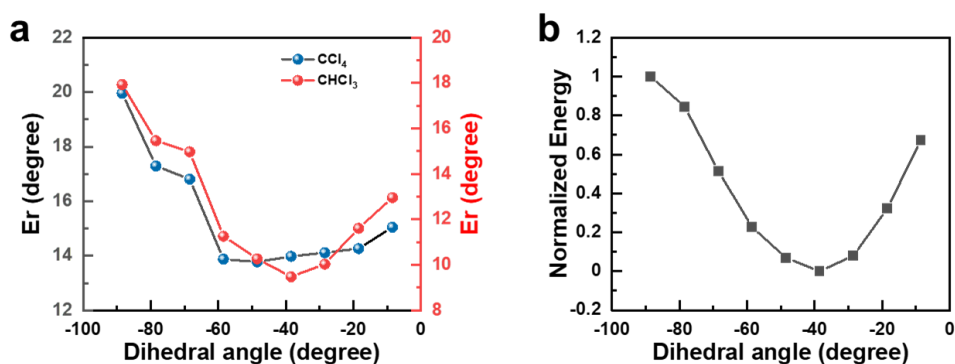
Fig.4 (a) Deviation Er's between the calculated and experimental vibrational cross angles and (b) the rescaled calculated energy vs the C-C(NDI)/C-S(Thiophene) dihedral angle in CCl_4 and $CHCl_3$.
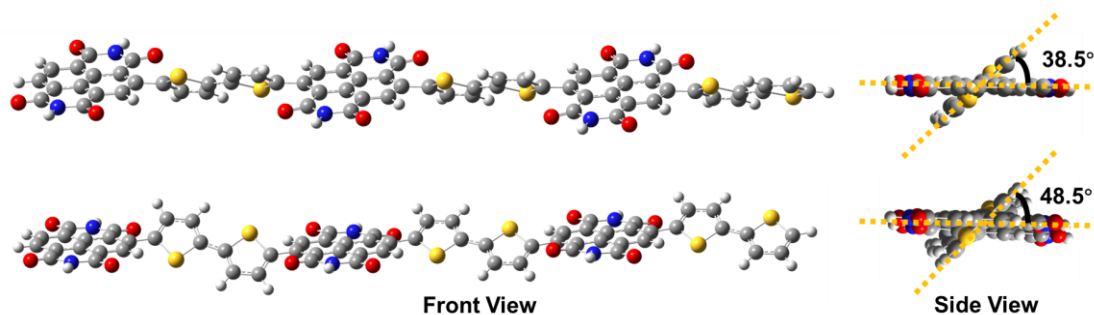

Fig.5 The most probable average molecular conformations in $CHCl_3$ (top) and CCl_4 (bottom) determined. The side views display the angles between the thiophene ring and the NDI skeleton.

We also study the polymer conformations in its solid films. It is interesting that films cast from both $CHCl_3$ and CCl_4 solutions have very similar vibrational cross angles, implying that both films have similar molecular conformations and morphology.

The experimental vibrational anisotropy and cross angle data of a solid film cast from a $CHCl_3$ solution are listed in table 2. Those of film from a CCl_4 solution are listed in SI. The observation is somewhat surprising. Previous research on other polymer films grown from different solutions suggested that the molecular morphology in solid films is often dependent on the selection of solvent.([20, 52, 59]) The crystalline structures and conformations of small organic molecules in solid films grown from different solutions can also be very different, even if the molecular conformations in the solvents are identical([60]). Although our result on the two polymer films seems anti-intuitive, a previous study on the same polymer using different experimental techniques including UV-Vis absorption and photoluminescence spectroscopy also suggested that its solid films cast from solutions with solvents of different polarity owned a similar morphology.([24]) Consistent with the vibrational cross angle measurements and previous work,([24]) UV-Vis absorption spectra of the polymer films cast from both $CHCl_3$ and CCl_4 solutions (fig.s9 in SI) are similar to those of the solutions except broader linewidths which are generally expected for solid samples because of reasons like inhomogeneity. The origin for the independence of film morphology on solvent was previously suggested([24]) to be that the film growth involves polymer chain aggregation in the solution within individual coils progressively shrinking upon decreasing the amount of solvent molecules during drying, and the rearrangement of polymer chains in the final stage of drying is likely to be insignificant. Base on this argument, one would expect the molecular conformations in solid films to be most similar to those in solutions with the least polar solvent where the polymer has most aggregates. However, vibrational cross angle measurements suggest a different direction. The vibrational cross angles of the solid films (table 2 and table S1 in SI) are very similar to those of the $CHCl_3$ solution rather than the CCl_4 solution (table 1). The result indicates that during drying the polymer chains do rearrange and they tend to form a more stable conformation for individual chains which are forced to aggregate into an energy-cost conformation by solvent CCl_4 in the CCl_4 solution. In other words, it also implies that the polymer solvates itself better than CCl_4, which is probably

because of the polar groups like C=O on the chain backbone that can interact with each other stronger than interact with the nonpolar CCl_4.

Table 2. Anisotropy and corresponding transition dipole moment cross angle between coupled vibrational modes of N2200 solid film cast from a $CHCl_3$ solution.

Pair Number	Coupled modes	Anisotropy	Cross angle
5	Thiophene Skeleton / NDI skeleton	0.36	15
6	Thiophene Skeleton / C=O(ν_{as-1})	0.3	24
7	Thiophene Skeleton / C=O(ν_{as-2})	0.08	47
8	NDI skeleton / C=O(ν_{as-1})	0.21	34
9	NDI skeleton / C=O(ν_{as-2})	-0.02	57
10	C=O(ν_{as-1}) / C=O(ν_{as-2})	-0.07	62

IV Concluding Remarks

In summary, the molecular conformations of a high-mobility n-type low-bandgap copolymer N2200 dissolved in $CHCl_3$ and CCl_4 and in solid films cast from both solutions are investigated with a ps/fs synchronized 2D IR technique by the vibrational cross angle method. In CCl_4 the polymer forms more aggregates and folds more and the backbone dihedral angle of C-C(NDI)/C-S(Thiophene) of its average conformation is about 10° more distorted than that in $CHCl_3$ and the most stable conformation for a free molecule. Anti-intuitively, the solid films cast from both solutions have the same molecular conformation, and the conformation is similar to that in the polar $CHCl_3$ rather than the conformation in the less polar CCl_4. The results imply that the interaction between polymer backbones (particularly through the polar C=O groups) is probably stronger than its interaction with CCl_4, which can naturally guide the rearrangement of polymer chains during the evaporation of solvent molecules. This work also implies that the balance and competition between the polymer/polymer interaction and the polymer/solvent interaction seems to be the dominant factor responsible for what morphology can form in a solid film cast from solution. It is not always true that different molecular conformations must exist in solid films grown from different

solutions with different polarity or different extents of aggregates with different conformations.

Supplementary information is available in the online version of the paper.

Author contributions

J.Z. and J.G. designed experiments. J.Z. and J.G. supervised the project. J.G., X.L., Z.Y. and J.Z. performed ultrafast experiments. J.G., X.L. and J.Z. analyzed data. C.S. conducted theoretical calculations. J.Z. and J.G., X.L. prepared and revised the manuscript.

Data availability statement

The data that supports the findings of this study are available within the article and its supplementary material.
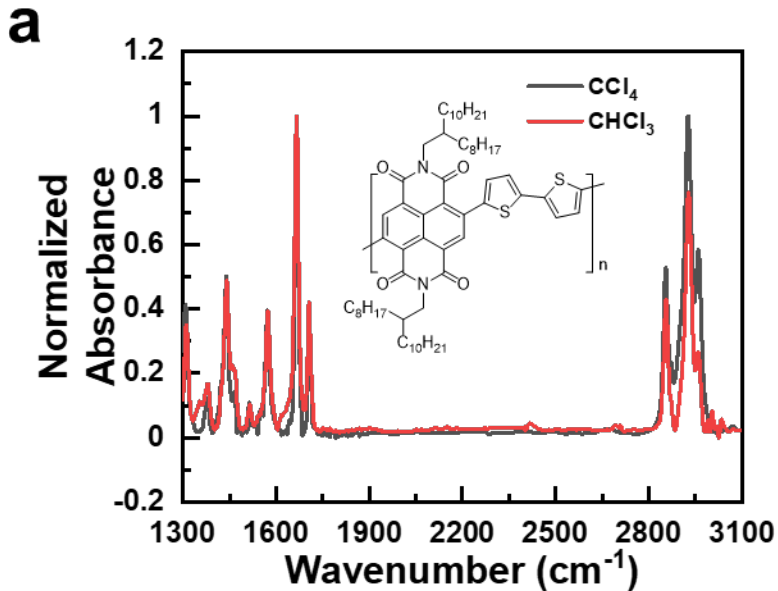
References:

1. S. Inal, J. Rivnay, A.-O. Suiu, G. G. Malliaras, I. McCulloch, Conjugated Polymers in Bioelectronics. *Acc. Chem. Res.* **51**, 1368-1376 (2018).
2. D. Dang, D. Yu, E. Wang, Conjugated Donor–Acceptor Terpolymers Toward High-Efficiency Polymer Solar Cells. *Adv. Mater.* **31**, 1807019 (2019).
3. P. M. Beaujuge, J. M. J. Fréchet, Molecular Design and Ordering Effects in π-Functional Materials for Transistor and Solar Cell Applications. *J. Am. Chem. Soc.* **133**, 20009-20029 (2011).
4. D. Venkateshvaran *et al.*, Approaching disorder-free transport in high-mobility conjugated polymers. *Nature* **515**, 384-388 (2014).
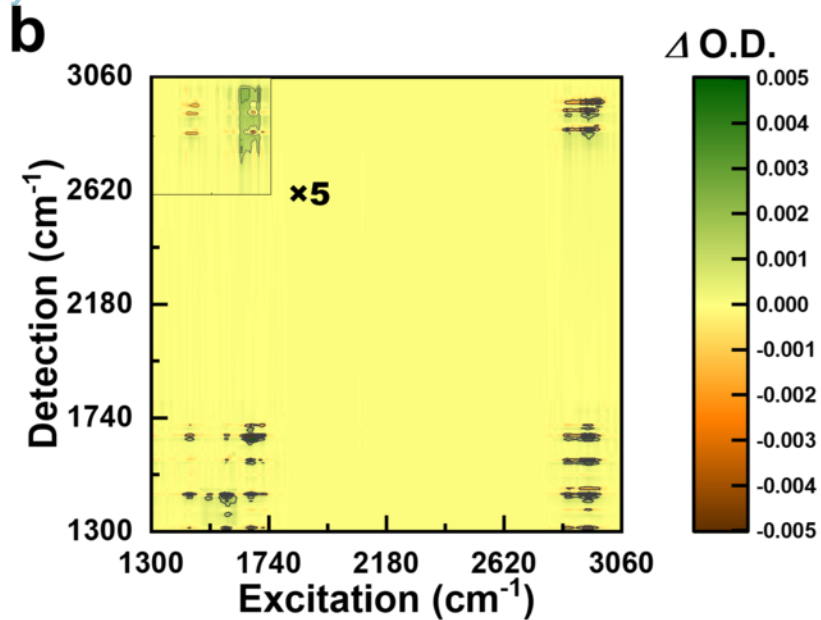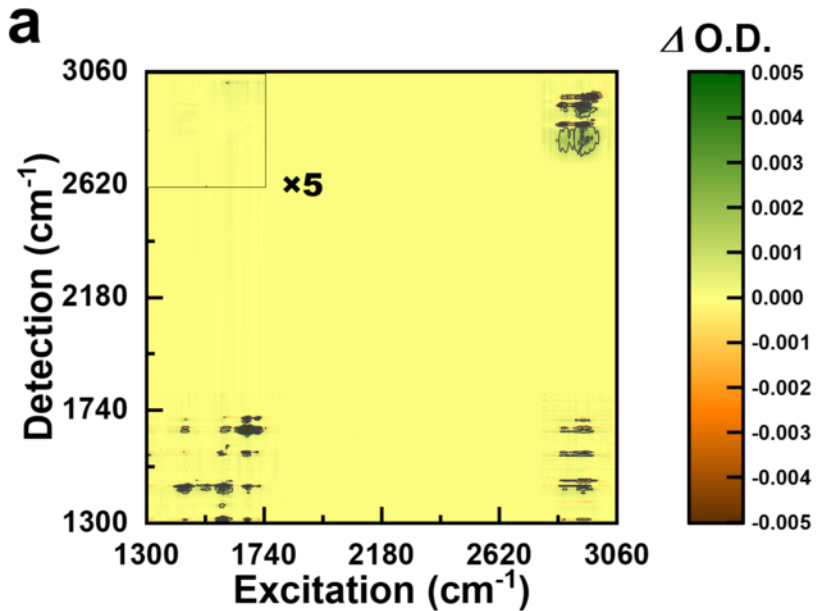
5.   K. S. Park, J. J. Kwok, P. Kafle, Y. Diao, When Assembly Meets Processing: Tuning Multiscale Morphology of Printed Conjugated Polymers for Controlled Charge Transport. *Chem. Mater.* **33**, 469-498 (2021).

6.   C. L. Donley *et al.*, Effects of Packing Structure on the Optoelectronic and Charge Transport Properties in Poly(9,9-di-n-octylfluorene-alt-benzothiadiazole). *J. Am. Chem. Soc.* **127**, 12890-12899 (2005).

7.   R. J. Kline *et al.*, Dependence of Regioregular Poly(3-hexylthiophene) Film Morphology and Field-Effect Mobility on Molecular Weight. *Macromolecules* **38**, 3312-3319 (2005).

8.   H. Sirringhaus *et al.*, Two-dimensional charge transport in self-organized, high-mobility conjugated polymers. *Nature* **401**, 685-688 (1999).

9.   S. Ning *et al.*, π-Conjugated Unit-Dependent Optical Properties of Linear Conjugated Oligomers. *Chin. J. Chem. Phys.* **27**, 315-320 (2014).

10.   C. Qing, W. Qing-zhen, Electrochemical Synthesis and Research of Two Polymers Composed of Alternate Carbazole and Thiophene Units. *Chin. J. Chem. Phys.* **28**, 639-644 (2015).

11.   L. Ding *et al.*, Controllable Transformation between the Kinetically and Thermodynamically Stable Aggregates in a Solution of Conjugated Polymers. *Macromolecules* **54**, 5815-5824 (2021).

12.   Y. Liu *et al.*, Aggregation and morphology control enables multiple cases of high-efficiency polymer solar cells. *Nat. Commun.* **5**, 5293 (2014).

13.   Y. Xi, C. M. Wolf, L. D. Pozzo, Self-assembly of donor–acceptor conjugated polymers induced by miscible 'poor' solvents. *Soft Matter* **15**, 1799-1812 (2019).

14.   J. Zhao *et al.*, Efficient organic solar cells processed from hydrocarbon solvents. *Nature Energy* **1**, 15027 (2016).

15.   K. S. Park *et al.*, Tuning conformation, assembly, and charge transport properties of conjugated polymers by printing flow. *Science Advances* **5**, eaaw7757.

16.   Z.-F. Yao *et al.*, Wafer-Scale Fabrication of High-Performance n-Type Polymer Monolayer Transistors Using a Multi-Level Self-Assembly Strategy. *Adv. Mater.* **31**, 1806747 (2019).

17.   Y.-Q. Zheng *et al.*, Unraveling the Solution-State Supramolecular Structures of Donor–Acceptor Polymers and their Influence on Solid-State Morphology and Charge-Transport Properties. *Adv. Mater.* **29**, 1701072 (2017).

18.   N.-K. Kim *et al.*, High-Performance Organic Field-Effect Transistors with Directionally Aligned Conjugated Polymer Film Deposited from Pre-Aggregated Solution. *Chem. Mater.* **27**, 8345-8353 (2015).

19.   Z.-F. Yao *et al.*, Ordered Solid-State Microstructures of Conjugated Polymers Arising from Solution-State Aggregation. *Angew. Chem. Int. Ed.* **59**, 17467-17471 (2020).

20.   Y. Jiang *et al.*, Fast Deposition of Aligning Edge-On Polymers for High-Mobility Ambipolar Transistors. *Adv. Mater.* **31**, 1805761 (2019).

21.   J. Rivnay *et al.*, Unconventional Face-On Texture and Exceptional In-Plane Order of a High Mobility n-Type Polymer. *Adv. Mater.* **22**, 4359-4363 (2010).

22.   T. Schuettfort *et al.*, Surface and Bulk Structural Characterization of a High-Mobility Electron-Transporting Polymer. *Macromolecules* **44**, 1530-1539 (2011).

23.   J. Rivnay *et al.*, Drastic Control of Texture in a High Performance n-Type Polymeric Semiconductor and Implications for Charge Transport. *Macromolecules* **44**, 5246-5255
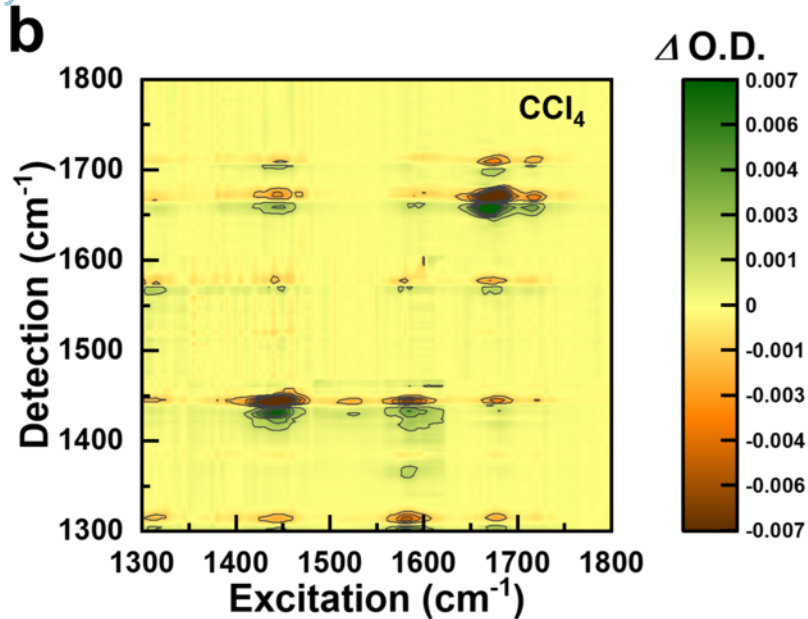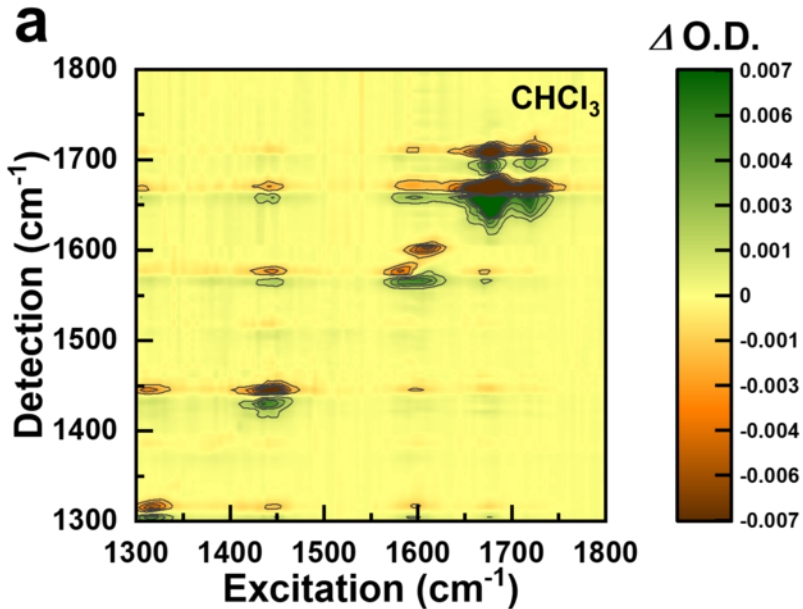
(2011).

24. R. Steyrleuthner *et al.*, Aggregation in a High-Mobility n-Type Low-Bandgap Copolymer with Implications on Semicrystalline Morphology. *J. Am. Chem. Soc.* **134**, 18303-18317 (2012).

25. H. Yan *et al.*, A high-mobility electron-transporting polymer for printed transistors. *Nature* **457**, 679-686 (2009).

26. J. Zheng, K. Kwak, M. D. Fayer, Ultrafast 2D IR Vibrational Echo Spectroscopy. *Acc. Chem. Res.* **40**, 75-83 (2007).

27. N. T. Hunt, 2D-IR spectroscopy: ultrafast insights into biomolecule structure and function. *Chem. Soc. Rev.* **38**, 1837-1848 (2009).

28. Z. Ganim *et al.*, Amide I Two-Dimensional Infrared Spectroscopy of Proteins. *Acc. Chem. Res.* **41**, 432-441 (2008).

29. J. Zheng *et al.*, Ultrafast Dynamics of Solute-Solvent Complexation Observed at Thermal Equilibrium in Real Time. *Science* **309**, 1338-1343 (2005).

30. J. Zheng, K. Kwak, X. Chen, J. B. Asbury, M. D. Fayer, Formation and Dissociation of Intra−

    Intermolecular Hydrogen-Bonded Solute−Solvent Complexes: Chemical Exchange

    Two-Dimensional Infrared Vibrational Echo Spectroscopy. *J. Am. Chem. Soc.* **128**, 2977-2987 (2006).

31. S. Y. Chun *et al.*, Direct observation of protein structural transitions through entire amyloid aggregation processes in water using 2D-IR spectroscopy. *Chem. Sci.* **13**, 4482-4489 (2022).

32. Y. Zhang *et al.*, Structural analysis of transient reaction intermediate in formic acid dehydrogenation catalysis using two-dimensional IR spectroscopy. *Proc. Natl. Acad. Sci. U.S.A.* **115**, 12395-12400 (2018).

33. P. Hamm, M. Lim, W. F. DeGrado, R. M. Hochstrasser, The two-dimensional IR nonlinear spectroscopy of a cyclic penta-peptide in relation to its three-dimensional structure. *Proc. Natl. Acad. Sci. U.S.A.* **96**, 2036-2041 (1999).

34. D. V. Kurochkin, S. R. G. Naraharisetty, I. V. Rubtsov, A relaxation-assisted 2D IR spectroscopy method. *Proc. Natl. Acad. Sci. U.S.A.* **104**, 14209-14214 (2007).

35. S.-H. Shim, M. T. Zanni, How to turn your pump–probe instrument into a multidimensional spectrometer: 2D IR and Vis spectroscopiesvia pulse shaping. *Phys. Chem. Chem. Phys.* **11**, 748-761 (2009).

36. M. F. DeCamp *et al.*, Amide I Vibrational Dynamics of N-Methylacetamide in Polar Solvents: The Role of Electrostatic Interactions. *The Journal of Physical Chemistry B* **109**, 11016-11026 (2005).

37. H. Maekawa, M. De Poli, C. Toniolo, N. H. Ge, Couplings between Peptide Linkages across a 3(10)-Helical Hydrogen Bond Revealed by Two-Dimensional Infrared Spectroscopy. *Journal of the American Chemical Society* **131**, 2042-+ (2009).

38. L. van Wilderen, D. Kern-Michler, H. M. Muller-Werkmeister, J. Bredenbeck, Vibrational dynamics and solvatochromism of the label SCN in various solvents and hemoglobin by time dependent IR and 2D-IR spectroscopy. *Physical Chemistry Chemical Physics* **16**, 19643-19653 (2014).
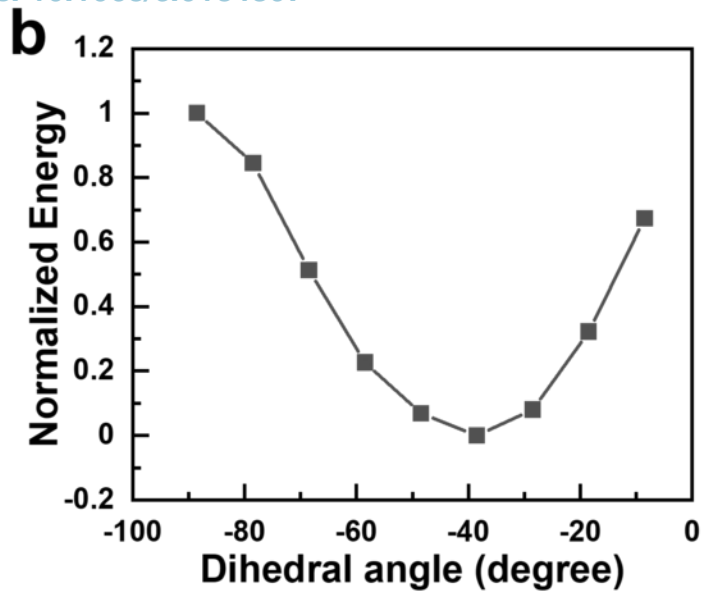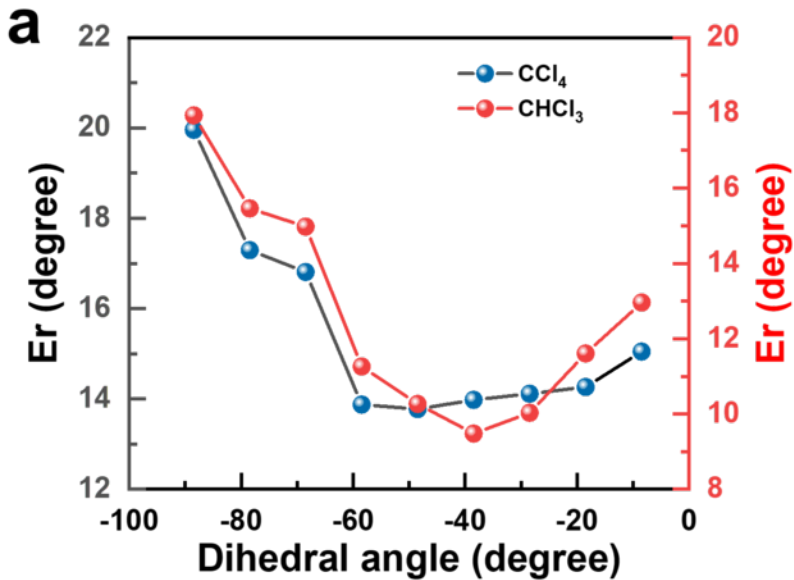
39.   J. T. King, M. R. Ross, K. J. Kubarych, Water-Assisted Vibrational Relaxation of a Metal Carbonyl Complex Studied with Ultrafast 2D-IR. *J. Phys. Chem. B* **116**, 3754-3759 (2012).

40.   B. Xiang *et al.*, Two-dimensional infrared spectroscopy of vibrational polaritons. *Proc. Natl. Acad. Sci. U.S.A.* **115**, 4845-4850 (2018).

41.   C. R. Baiz, D. Schach, A. Tokmakoff, Ultrafast 2D IR microscopy. *Opt. Express* **22**, 18724-18735 (2014).

42.   T. I. C. Jansen, S. Saito, J. Jeon, M. Cho, Theory of coherent two-dimensional vibrational spectroscopy. *J. Chem. Phys.* **150**, 100901 (2019).

43.   S. T. Roberts, J. J. Loparo, A. Tokmakoff, Characterization of spectral diffusion from two-dimensional line shapes. *J. Chem. Phys.* **125**, 084502 (2006).

44.   H. Chen *et al.*, Vibrational Cross-Angles in Condensed Molecules: A Structural Tool. *J. Phys. Chem. A* **117**, 8407-8415 (2013).

45.   H. Chen, H. Bian, J. Li, X. Wen, J. Zheng, Relative Intermolecular Orientation Probed via Molecular Heat Transport. *J. Phys. Chem. A* **117**, 6052-6065 (2013).

46.   J. Bredenbeck, J. Helbing, C. Kolano, P. Hamm, Ultrafast 2D–IR Spectroscopy of Transient Species. *ChemPhysChem* **8**, 1747-1756 (2007).

47.   J. D. Cyran, A. T. Krummel, Probing structural features of self-assembled violanthrone-79 using two dimensional infrared spectroscopy. *J. Chem. Phys.* **142**, 212435 (2015).

48.   H. Bian *et al.*, Mapping Molecular Conformations with Multiple-Mode Two-Dimensional Infrared Spectroscopy. *J. Phys. Chem. A* **115**, 3357-3365 (2011).

49.   H. Chen, H. Bian, J. Li, X. Wen, J. Zheng, Ultrafast multiple-mode multiple-dimensional vibrational spectroscopy. *Int. Rev. Phys. Chem.* **31**, 469-565 (2012).

50.   S. Nigam, S. Rutan, Principles and applications of solvatochromism. *Appl. Spectrosc.* **55**, 362a-370a (2001).

51.   P. Suppan, Invited review solvatochromic shifts: The influence of the medium on the energy of electronic states. *Journal of Photochemistry and Photobiology A: Chemistry* **50**, 293-330 (1990).

52.   T.-Q. Nguyen, V. Doan, B. J. Schwartz, Conjugated polymer aggregates in solution: Control of interchain interactions. *J. Chem. Phys.* **110**, 4068-4078 (1999).

53.   M. Grell *et al.*, Chain geometry, solution aggregation and enhanced dichroism in the liquidcrystalline conjugated polymer poly(9,9-dioctylfluorene). *Acta Polym.* **49**, 439-444 (1998).

54.   M. Khalil, N. Demirdoven, A. Tokmakoff, Coherent 2D IR Spectroscopy: Molecular Structure and Dynamics in Solution. *J. Phys. Chem. A.* **107**, 5258-5279 (2003).

55.   J. Zheng *et al.*, Accidental vibrational degeneracy in vibrational excited states observed with ultrafast Two-Dimentional IR vibrational echo spectroscopy. *J. Chem. Phys.* **123**, 164301 (2005).

56.   J. Zheng, *Ultrafast Chemical Exchange Spectroscopy.*   (VDM Verlag, 2008), pp. 216.

57.   Y. Futami, Y. Ozaki, Y. Hamada, M. J. Wojcik, Y. Ozaki, Solvent Dependence of Absorption Intensities and Wavenumbers of the Fundamental and First Overtone of NH Stretching Vibration of Pyrrole Studied by Near-Infrared/Infrared Spectroscopy and DFT Calculations. *J. Phys. Chem. A* **115**, 1194-1198 (2011).

58.   H. L. Chen, H. T. Bian, J. B. Li, X. W. Wen, J. R. Zheng, Ultrafast multiple-mode multiple-dimensional vibrational spectroscopy. *Int. Rev. Phys. Chem.* **31**, 469-565 (2012).
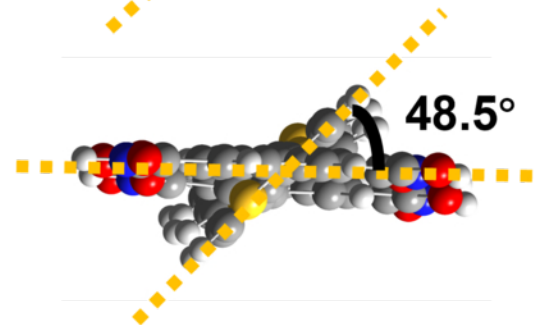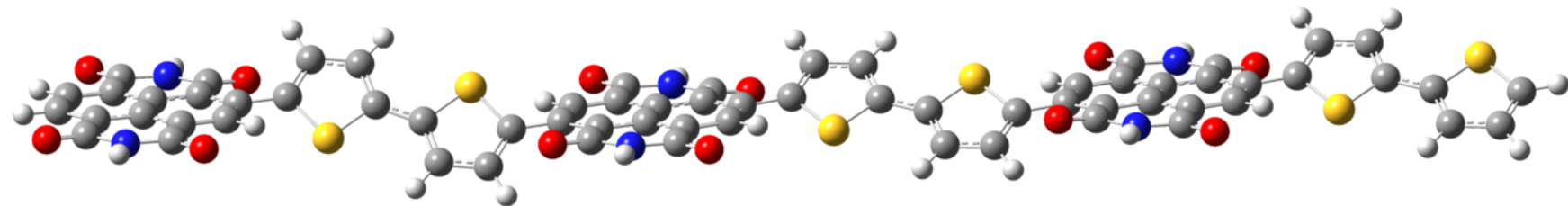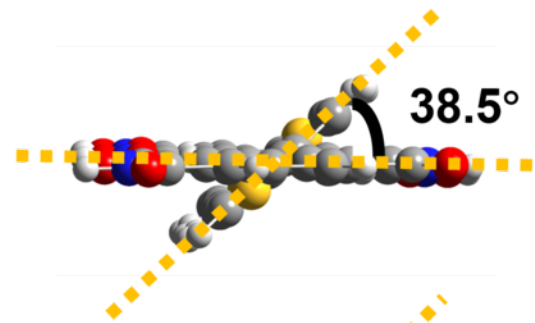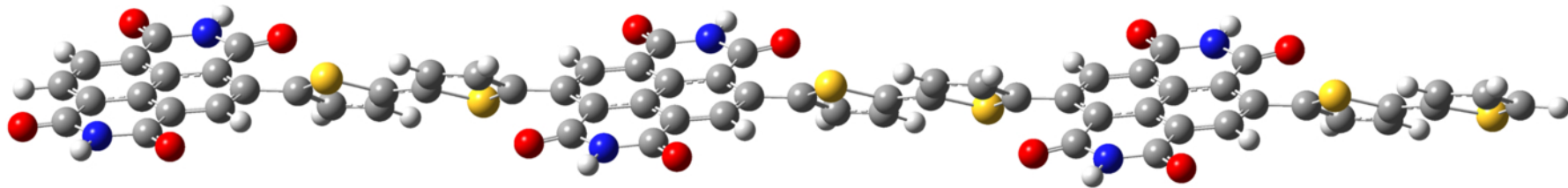
59.   S. Berson, R. De Bettignies, S. Bailly, S. Guillerez, Poly(3-hexylthiophene) Fibers for Photovoltaic Applications. *Adv. Funct. Mater.* **17**, 1377-1384 (2007).

60.   H. Chen *et al.*, Vibrational Cross-Angles in Condensed Molecules: A Structural Tool. *J. Phys. Chem. A* **117**, 8407-8415 (2013).

Front View

Side View

38.5°

48.5°